# Chapter 6

# DLD for Size Profiling of Smaller Blood Cells

## 6.1 Introduction

This chapter examines the behaviour of the red blood cells and platelets in a deterministic lateral displacement (DLD) device with particular focus on platelets because of their complex and dynamic behaviour.

Platelet function is vital yet highly variable. Rapid platelet and clotting analysis for point of care diagnostics is a growing area of interest. While commercial products exist for platelet function analysis, no product meets all clinical needs. We demonstrate the effectiveness of a new, rapid microfluidic method for platelet size and morphology measurements in whole blood that may provide more detailed information than current methods. The device described here continuously separates particles by size. Particles are displaced laterally in proportion to their size in a micro-fabricated post array, allowing particle size to be determined from exit position. Whole blood, labeled with PE-anti-CD41[i], was run through the device and the

[i]CD41 binds to platelet surfaces.

positions of fluorescent objects noted as they exited the array. From this, size histograms are created. We show that platelet sizes increase after exposure to thrombin and $4^o$C. We also show that platelets are not activated, and that cells are not killed by passage through the microfluidic device.

This work follows in the footsteps of previous work using microfluidic devices to continuously separate particles, including blood, by size. Huang et al. [5] introduced the deterministic lateral displacement (DLD) method and showed astounding size resolution with polystyrene beads, while Davis et al. [47] recently gave a thorough demonstration of the method as applied to blood. Chapters 4 and 5 of this thesis show how to extend the range of the DLD method for blood filtration and how to use the method to measure the size of white blood cells. This work moves beyond previous work with blood [73] by focusing on platelets and showing clear differences in platelet size as a result of exposure to agonists. We will briefly describe the physics of the deterministic lateral displacement principle, then describe the device, followed by the results for platelets and red blood cells.

### 6.1.1 Platelet function and traditional testing

Hemostasis in humans is a vital process that has three functions: to maintain blood as a fluid while circulating, to stop bleeding and blood loss at the site of injury by forming a clot, and to ensure the eventual removal of the clot once healing is complete. This requires holding a balance between conflicting tendencies where any exaggeration or deficiency in one can lead to excessive clotting or bleeding [74].

Platelets are one component of the hemostatic system. In the blood they are small enucleated (no nucleus) discs. Frojmovic et al. [75,76] made optical measurements of citrate-anticoagulated, fixed, freely rotating platelets in citrate-anticoagulated blood. In two separate studies, they measured the large diameters to be $3.6 \pm 0.7\mu$m and $3.2 \pm 0.5\mu$m, and the thickness to be $0.92 \pm 0.34\mu$m and $1.1 \pm 0.2\mu$m, respectively, with

greater than 80% of platelets having the discoid shape. Some 2 to 10% of the platelets were echinocytes, spherical objects with irregular surfaces and spiny or tenticle-like objects extending from the cell (pseudopods), with the remainder being "irregular forms." On dried blood smears, platelets appear smaller, 2 to 3 $\mu$m in diameter [77].

Platelets function by aggregating and adhering to tissue, a central component of the clotting process. During aggregation, platelets change shape from discocytes to echinocytes and experience a host of physiochemical changes; this process is collectively called activation.

Diagnosing platelet function and condition can help to assess a person's risk of excessive bleeding prior to surgery, help monitor a patient's response to certain blood disorder and cardiology drugs, and can determine the viability of platelets for transfusions. There are numerous tests for platelet function. Traditional tests include measurements of bleeding time, aggregation in response to agonists, chemical detection methods, electron microscopy, high-shear platelet function, and retraction forces during clotting [78]. Various new platelet function tests are available to automate some of the traditional tests and measure new aspects of platelet function such as protein and mRNA content [78]. Flow cytometry is also being used to analyze platelets. While many of the new platelet function tests could be considered microfluidic, there are very few examples of platelet work in the common microfluidics literature [79,80].

Despite the importance of platelet morphology, the author is not aware of any automated systems to asses morphological changes. Electron microscopy gives the best picture of morphology, but sample sizes are low, the preparation required for imaging is extensive, and scanning electron microscopes are very expensive. Here we present a microfluidic device that measures platelet size. We demonstrate an increase in the apparent size of platelets after exposure to thrombin or refrigeration at $4^{\mathrm{O}}$ C. Given the well known morphological changes that occur during refrigeration [81], we hypothesize that the increase in "hydrodynamic size" is a result of a morphological

| $\epsilon$ | Post Diameter | Gap | Length of Section | Lateral Displacement |
|---|---|---|---|---|
| 1/42 | 20 | 17 | 7308 | -222 |
| 1/100 | 20 | 6 | 7800 | 78 |
| 1/50 | 20 | 6 | 2600 | 52 |
| 1/29 | 20 | 6 | 2263 | 78 |
| 1/22 | 20 | 6 | 1145 | 52 |
| 1/18 | 20 | 6 | 937 | 52 |
| 1/15 | 20 | 6 | 780 | 52 |
| 1/12 | 20 | 6 | 624 | 52 |
| 1/10 | 20 | 6 | 520 | 52 |
| 1/8 | 20 | 6 | 415 | 52 |
| 1/12 | 20 | 8 | 672 | 84 |
| 1/10 | 20 | 8 | 559 | 84 |

Table 6.1: Device specifics as in L-Edit (Tanner EDA, CA USA) mask file "Mid-Range_histogramer_V1_ready.tdb". The separation column in the first section is 1160 $\mu$m wide. The separation column in the platelet fractionation array is 885$\mu$m wide. Dimensions in the table are microns.

change. In this work, size is used to refer to a linear dimension, rather than volume.

## 6.2 Methods

As described in Chapters 3 and 4 there is a limit to the range of particle sizes that can be separated in a single array. In order to separate red blood cells and platelets, the larger white blood cells must be prevented from clogging the separation array. Upstream of the platelet fractionation array we use another array to divert particles larger than 5 microns into an alternate non-clogging path, allowing the smaller particles (platelets and red blood cells) to be fractionated in an array that runs parallel to the alternate non-clogging path. The first section and the alternate path have a gap of 17 and 20 microns respectively. The platelet fractionation array has a minimum gap of 6 microns. The platelet fractionation array is composed of a series of arrays, each with increasing critical particle size so that increasing lateral displacement correlates with increasing size.

Table 6.1 give details of the array. The entire device fits on a standard glass slide;

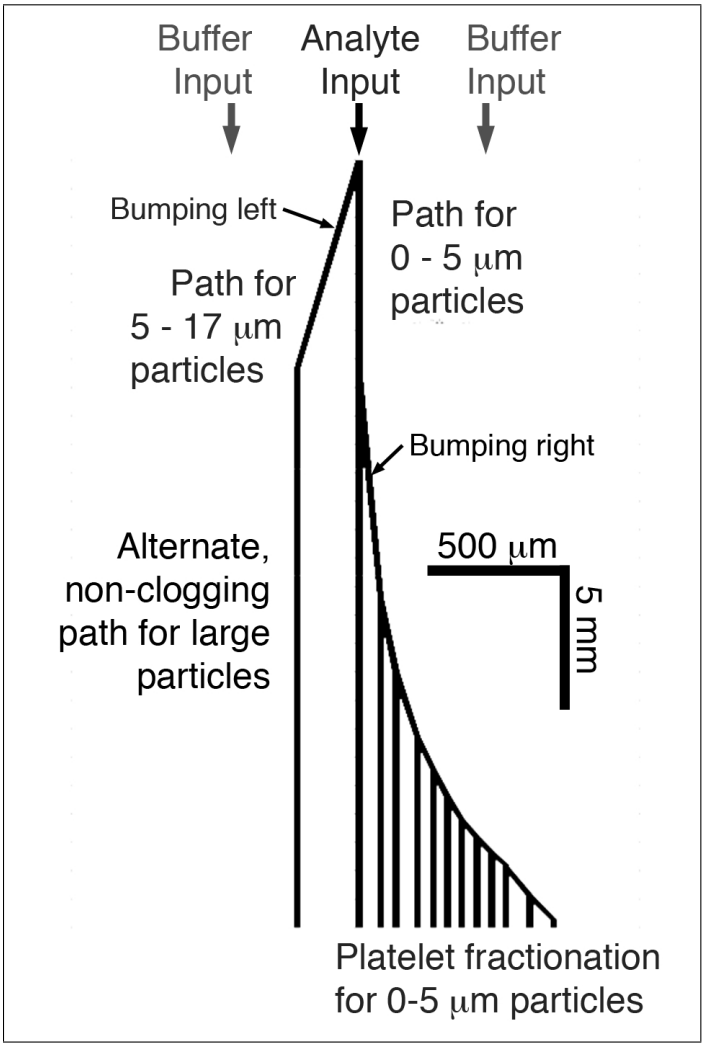


Figure 6.1: Diagram of ideal particle paths, compressed vertically 10 times. Particles that would clog the lower portion of the device are moved left into a 20-micron gap channel that runs parallel to but is not in connection with the platelet fractionation array. In the platelet fractionation array, increasing lateral displacement correlates with increasing size.

The distance between the buffer input and the outputs is 6.3 cm. Figure 6.1 shows the ideal paths for all particles that enter the device as they branch off of the narrow input stream. Particles larger than 17 microns are sufficiently rare in blood not to cause any apparent jamming or build up in any part of the device. Figure 6.2 shows a detailed image from the mask layout software of the transition between the first and second sections. It shows how particles greater than 5 microns are separated from the smaller particles and flow into the alternate non-clogging path. The pressure drop through the alternate non-clogging path has been designed so that the flow profile in the separations arrays remains vertical.

The device consists of a PDMS mold sealed to a fluorosilane-coated silicon wafer

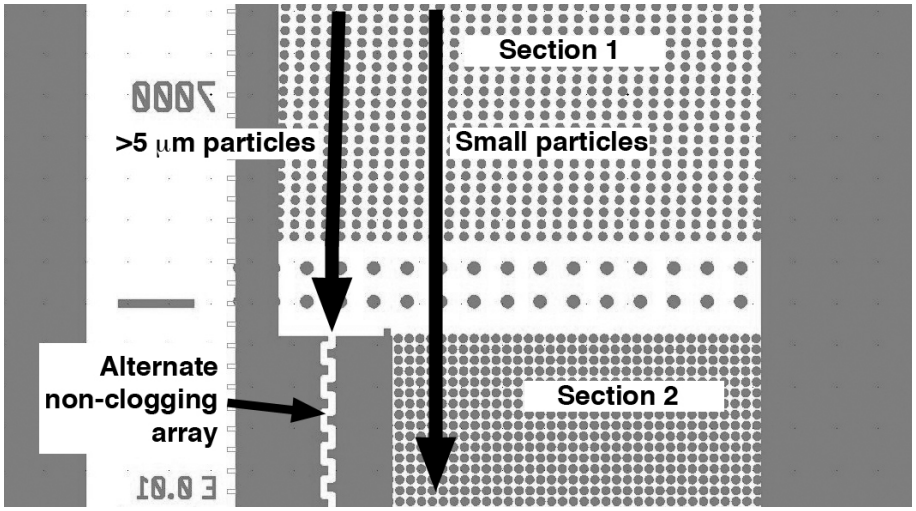


Figure 6.2: Image from the mask layout software of the transition between the first and second sections. Arrows indicate the paths of large and small particles. The gaps in the first section are 17 microns and in the second section are 6 microns.

backplane that had been cleaved to the size of a standard glass slide. The mold was created by standard photolithography on a silicon substrate, followed by an 18 micron deep silicon etch. This was cleaned, baked at 1000 $^{o}$C for 3 hours, and coated with a fluorosilane. PDMS was poured over the master mold and squished under a 2.5 by 7.5 cm glass slide, then allowed to cure for 2 hours at 70 $^{o}$C. The PDMS-coated glass slide was separated from the master mold using a razor blade and sealed to the backplane. Holes for fluid connections had been sandblasted into the silicon wafer backplane. After assembly the chip is soaked in a solution of DI water containing 2 g/l pluronic F108 (BASF) and placed under vacuum for at least 2 hours to remove trapped air bubbles from within the device.

All experiments were done using chips fabricated at Princeton University. Etching was performed by Keith Morton. Experiments using blood were performed at Princeton University and at the Wadsworth Center of the New York State Department of Health in collaboration with Dr. David Lawrence. Flow cytometry was performed at Princeton University with the help of Christina DeCoste, and at the Wadsworth Center with the help of Renj Song and Joan Peterson-Lane.

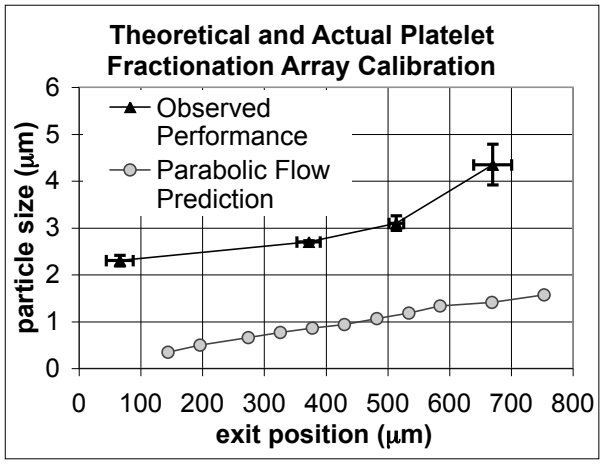


Figure 6.3: Plot of the particle size vs the exit position (measured from the left column edge) for the platelet fractionation array. Horizontal error bars are one standard deviation in each direction, as determined by fitting a gaussian to the fluorescence intensity profiles (not shown). Vertical error bars are determined from the coefficient of variation specified by the manufacturer. The observed critical particle sizes are much larger than that predicted by parabolic flow in the gaps with overall vertical flow.

Figure 6.3 shows plots of the critical particle sizes versus exit position in the platelet fractionation array for both the theory and experimental calibration using polystyrene beads of known and fixed size. The theoretical prediction is based on the assumption of parabolic flow and that the critical diameter is 2 times the width of the first streamline, as described in Chapter 3 and given in Figure 3.4. We observe critical particle sizes that are much larger than that predicted by any previous experience. This difference may be due to the combination of a large post to gap ratio (20:6) and a rhombic array (see section 3.4). Later versions of this device having a wider separation column (device walls moved out, further from blood injection point) showed no decrease in the critical particle sizes. Despite this surprising result the device does a fine job of separating platelets and red blood cells.

## 6.3 Experiments

Fluid is driven through the device by positive air pressure applied to both the buffer and blood input ports by an electronically controlled regulator. The running buffer was AutoMACS buffer (Miltenyi Biotech) with no additives. When whole blood

enters the device (either capillary or venous, EDTA-anticoagulated or ACD[ii]), all the white blood cells are diverted into the alternate non-clogging path (Fig 6.4 left image). White blood cells behave as particles larger than 5 microns in diameter in DLD arrays [47,73]. A fraction of platelets enter the alternate non-clogging pathway, and the remainder enter the platelet fractionation array. These "large" platelets are counted in the later histograms as greater than 4.8 $\mu$m in diameter

### 6.3.1 Platelet behavior

To determine platelet size distribution, fluid is driven through the device at 2 psi (14 kPa). This provides a suitable rate of cells for counting and a suitable residence time in front of the camera to be imaged. Five parts ACD whole blood are incubated with one part PE-conjugated antihuman CD41 (ebioscience.com), for 20 minutes at room temperature prior to running in the microdevice. No wash step is required at this concentration of label. The device is mounted on an inverted fluorescence microscope with high pressure mercury lamp illumination. Video is captured by a Hamamatsu silicon intensified-target video camera and recorded onto a Sony miniDV cassette recorder. This set-up is shown in the introduction, (Fig. 1.2).

We record the lateral positions of bright streaks at the end of the platelet fractionation array as the platelets travel through a set of 22, 40-micron period, parallel channels. The value plotted in the exit position histograms of Figures 6.7A and 6.8A represents the fraction of cells that travelled through each channel. In the same image we record cells that have travelled through the alternate non-clogging path; these cells are plotted at negative 50 microns on the horizontal axis. All charts are normalized.

[ii] Anticoagulant Citrate Dextrose

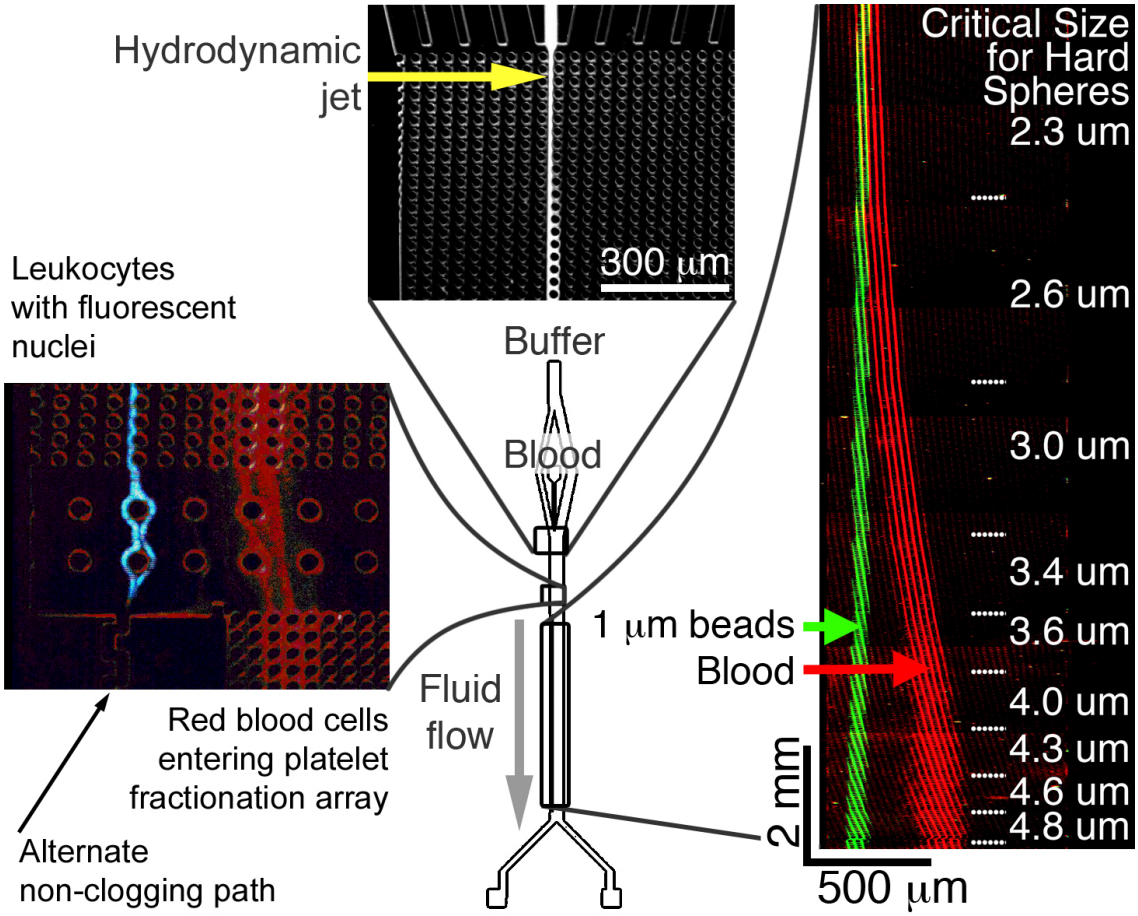


Figure 6.4: Micrographs of various particles in the device at three locations. In the device the fluid flows from top to bottom. TOP: A hydrodynamic jet of beads entering the first separation array. LEFT: White blood cells (blue) separated from other cells after the first separation array and immediately before entering the alternate non-clogging path. RIGHT: Overlay of separate images of a stream of 1-micron fluorescent beads (green) and whole blood (red). The 1-micron beads are not displaced by the separation array at any point. The image is compressed vertically 4 times. The numbers 2.3 to 4.8 are the approximate measured critical particle sizes. Notice that the whole blood, composed mostly of red blood cells, travels at an angle to the flow until the section with a 4-micron critical particle size.

### Thrombin induced platelet activation

In vivo, thrombin is released at the site of tissue damage and causes coagulation; it also de-solubilizes fibrin. We prepared control and thrombin-activated blood samples using the procedure given by Leytin et al. in 2000 [82][iii]. The activated sample is exposed to 1 NIH unit/ml of human thrombin (SigmaAldrich.com) and involves fixing both blood samples in paraformaldehyde. The control sample is not exposed to thrombin.

We verify activation in the same way as Leytin et al., by the expression of CD62p, who observed that with increasing doses of thrombin, on average, platelets bind more CD62p. Figure 6.5 shows the level of CD62p expression for the control and thrombin-activated populations as measured by flow cytometry. For flow cytometry, FITC-conjugated CD41 was used simultaneously to identify all platelets in whole blood. Activation is defined as events which are both $CD41^+$ and $CD62p^+$ (CD62p expression >294, as shown in Figure 6.5 and Figure 6.6). 99.9% of all non-platelet events ($CD41^-$) in similar tests recorded by the flow cytometer have a CD62p fluorescence value less than 294. These events represent the non-specific binding level of the CD62p antigen, so it makes a natural choice for the cut-off value. The CD41 cut-off value is 250, this lies in the middle of two clearly resolvable groups on the horizontal axis, CD41, in Figure 6.6.

These two samples were measured in the microfluidic device, without the platelet activation marker (CD62p). We created an exit position histogram for $CD41^+$ events, and observed an increase in hydrodynamic size in the sample treated with thrombin prior to putting the sample in the chip. Figure 6.7A shows the exit position histograms for 4 experiments, where the mean and standard deviation (as error bars) for each bin are plotted. Figure 6.7B shows the same data, re-binned to show the hydrodynamic

[iii]Leytin et al. gives a detailed description of the protocol which uses ACD blood mixed with the fibrin polymerization inhibitor GPRP (SigmaAldrich.com) to prevent aggregation.

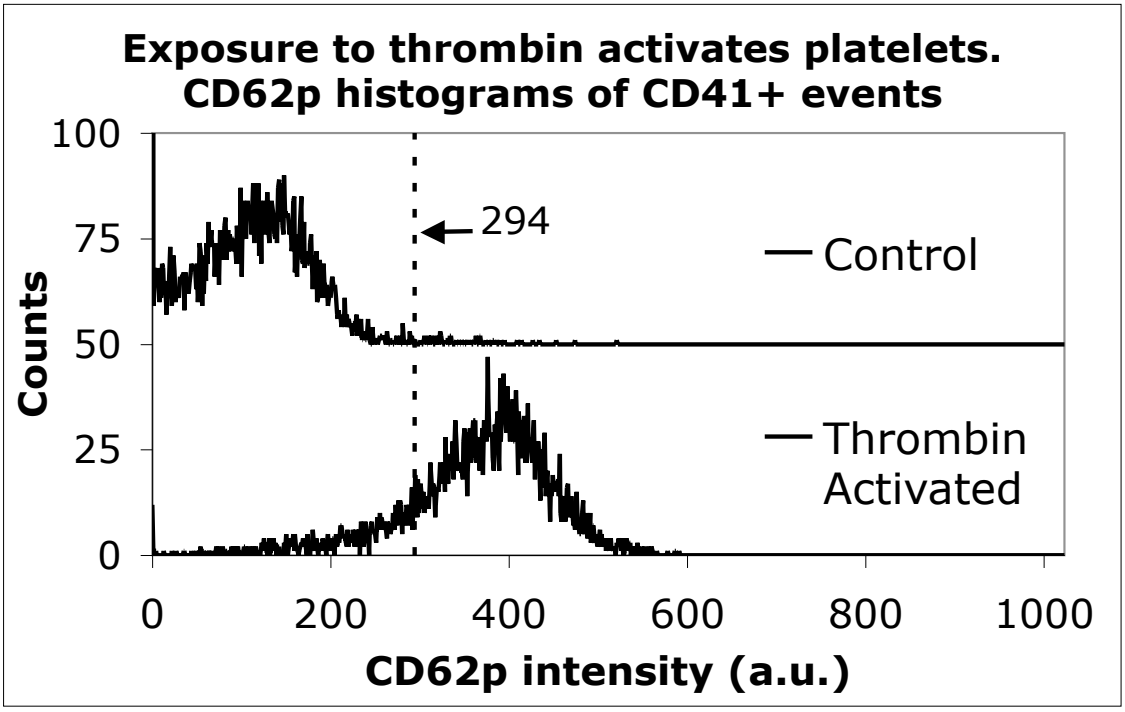


Figure 6.5: Thrombin treatment of whole blood causes activation of platelets, evaluated by CD62p expression of $CD41^+$ events in a FACScan flow cytometer. In the control sample, 1.1% of platelets are activated. In the thrombin-activated sample, 87% of platelets are activated.

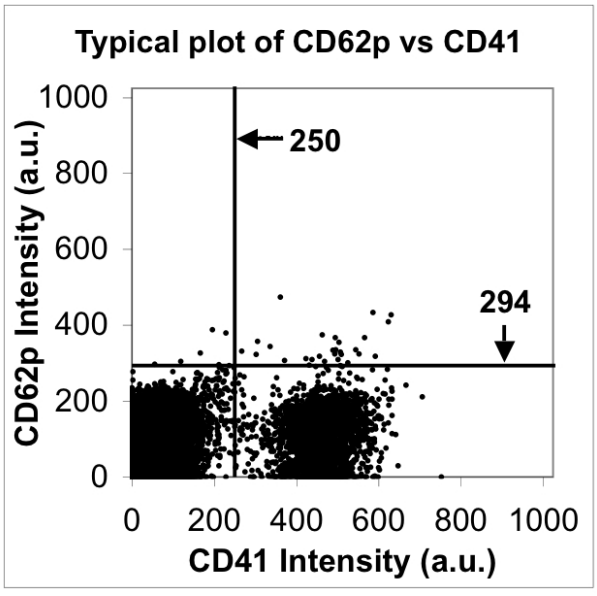


Figure 6.6: Typical plot of CD62p intensity vs CD41 intensity for non-activated blood samples. The CD41 gate (250) is used to decide whether an event is a platelet or not, while the CD62p gate (294) is used to decide whether the platelet event is activated.

size histogram. All data has been normalized, and more than 400 platelets were counted in each experiment. Each experiment takes between 1 and 2 minutes to collect the positions of the 400 platelets.

In the thrombin-activated sample there is a 10-fold reduction in the smallest platelets (under 2.4 $\mu$m in diameter), and a 2.5-fold increase in the number of platelets larger than 4.8 microns. We can calculate a mean using the centers of the hydrodynamic size bins (somewhat arbitrarily assuming the last bin is 4.8 to 7 $\mu$m). The hydrodynamic size of the control population platelets (3.1 $\mu$m) are similar to the large diameters of platelets measured by Frojmovic et al. in 1976 and 1978 [75,76] ($\sim 3.4\mu$m), see section 6.1.1. The activated sample measurement (mean size of 4.4$\mu$m) gives sizes that are larger than that reported by Frojmovic et al. It is possible that some of the largest objects are platelet-platelet and platelet-cell aggregates.

Numerous studies have been devoted to the analysis of platelet morphology changes. Activation involves a change from discoid state to spherical cells with pseudopods (spiny or tenticle-like projections from the cell wall) called echinocytes. Cold storage also causes activation and morphological changes, though these morphological changes are reversible upon re-warming [81]. The morphological changes are also experienced by nearly all platelets; Zucker et al. in 1954 reported the conversion of 95% of discoid platelets to spheroids, with the other 5% being difficult to classify. Upon re-warming, about 70% returned to a normal disc shape. By light microscopy, the transition from disc to sphere appears as a reduction in size, since in the disc shape, many cells present the viewer with their large diameters.

This leads to the question: Is there an increase in size upon activation? Using the Coulter principle, Bull et al. [84] observed an increase in platelet volume of 24% upon cold storage. Converting these volumes to spheres, the reported difference corresponds to a 180 nm increase in diameter on a 2.3 micron sphere, about 8%. A slightly smaller increase in volume was observed for platelets exposed to 10 units/mL thrombin. The

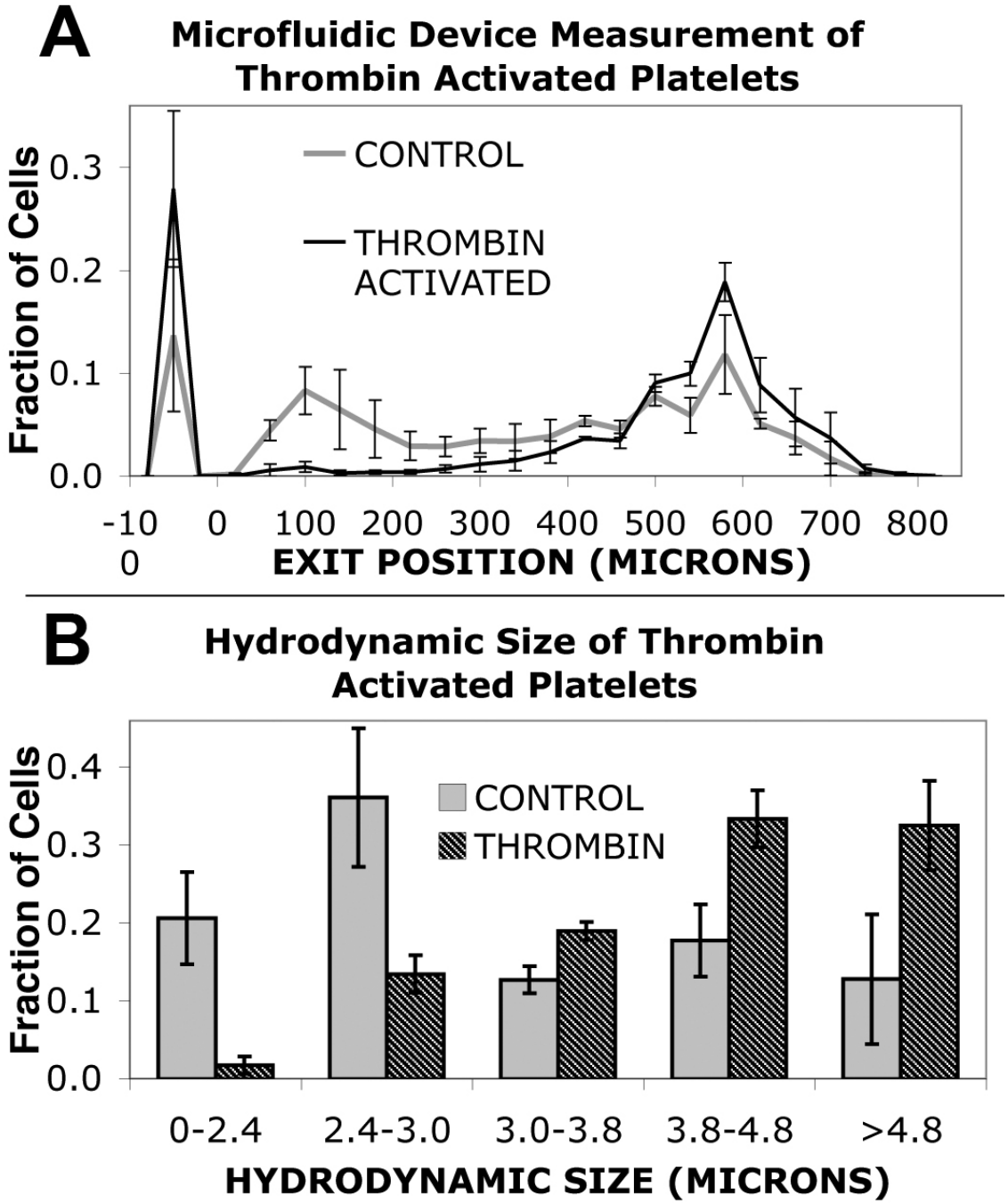


Figure 6.7: Microdevice exit position and hydrodynamic size histograms for control and thrombin-activated blood samples. A significant increase in size is observed after exposure to thrombin, without the use of an activation specific marker.

dominant morphological effect of exposure to either thrombin or cold temperatures is a change from discoid to spheroid with an irregular surface and pseudopods, and not an increase in overall size or volume.

**Temperature induced changes**

Similar data are obtained when our experiment is repeated with warm and cold blood. Here, the blood and the assembled and ready-to-run microfluidic device were, seperately, either refrigerated at $4^o$ C or placed in a $37^o$ C incubator for at least 30 minutes prior to running the experiment. Next, the above listed items are placed on the microscope (which is at room temperature), where the blood is loaded into the input well, and the external plumbing connected. The experiment was then immediately run, and completed within 3 minutes, thus giving the chip, blood, and liquids as little time as possible to return to room temperature. Reports [83] indicate that the activation-induced shape change is mostly complete after 10 minutes and complete after 30 minutes.

Figure 6.8 shows the exit positions histograms and hydrodynamic size histograms for the warm and cold platelets. The experiment was repeated two separate times, weeks apart, with blood from the same person. A total of 5 different microdevices were used. The error bars in (A) represent the standard deviation observed for each bin across all five experiments, in (B) they are the standard deviation of the re-grouped data.[iv]. As with thrombin exposure, the cooling induced morphological change is expressed as an increase in hydrodynamic size. There is a sharp reduction in the fraction of the smallest platelets and more than twice the number of the largest platelets. The mean sizes are 2.7 $\mu$m in the warmed sample and 4.0 $\mu$m in the chilled sample. This result is very similar to that observed when thrombin is used

[iv] exit positions 20-80 microns become 0-2.4 microns in hydrodynamic size; positions 100-480 become 2.4 to 3.0; positions 520-560 become 3.0-3.8; positions 600-680 become 3.8-4.8; positions 720-880 plus the negative 50 position becomes >4.8.

to activate the cells. This suggests that the morphologic change from discoid to spheroid, that is known to occur in both cases, is causing the change in hydrodynmic size. The increase in the fraction of large (>4.8) cells is not expected to be caused by aggregation as no evidence of aggregation is seen in the cited studies of temperature induced morphological changes.

### 6.3.2 Discussion

Comparing Figures 6.7 and 6.8, it is hard to miss the similarity. The control sample from the thrombin effect experiment, being done at room temperature, would fit nicely in between the curves for the warm and cold blood in Figure 6.8. The common thread in both experiments is a morphological change, and I believe that this is manifest as an increase in hydrodynamic size. Future work should look at Cd62p expression in the chip to see if $CD62p^+$ platelets exist mostly in the large size range. It is possible that the discocyte cell behaves as a particle with size proportional to its narrow dimension, and when it converts to a spherocyte with pseudopods the size increases. However this is hard to reconcile with the observation that most discoytes behave as particles greater than 2.4 microns thick, when 1 micron is their typical thickness. Some other interaction between the complex fluid flow field and the platelets shape may be causing this effect. Nevertheless the method appears capable of distinguishing and separating platelets based on morphology.

### 6.3.3 Possible microdevice-induced changes

Platelets are sensitive to a wide range of stimuli. Activation can be caused by cool temperatures, various chemicals including the anticoagulants that prevent clotting, thrombin, collagen, contact with certain surfaces like $SiO_2$ and high shear stress. Shear is the spatial derivative of velocity, $\vec{\bigtriangledown}V$, and has units of $s^{-1}$; it causes stretching forces on the cell membrane through the fluid viscosity. We have used a flow cytometer

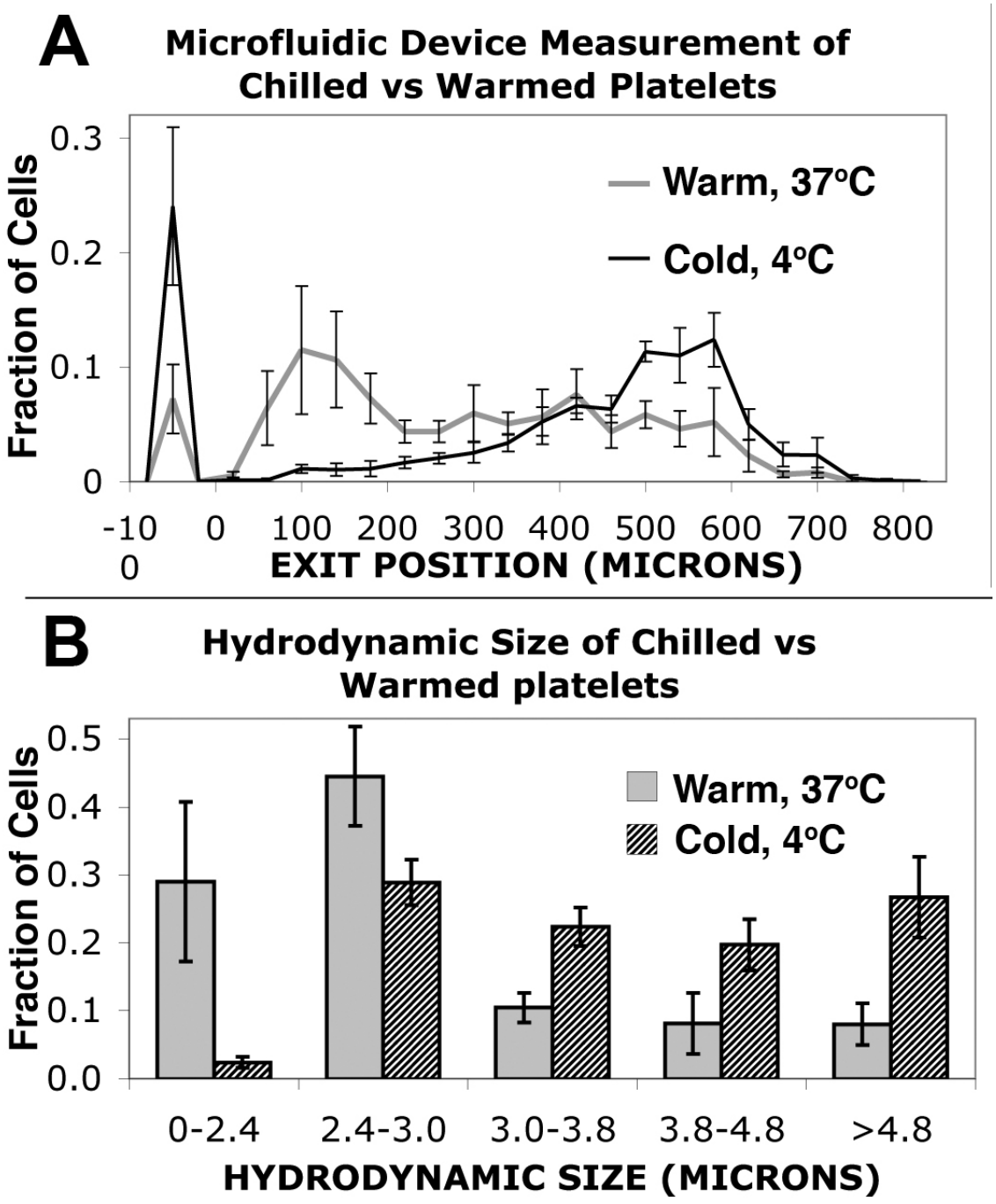


Figure 6.8: Exit position and hydrodynamic size histograms for chilled and warmed platelets in whole blood samples. A significant increase in hydrodynamic size is observed in the microfluidic device upon chilling, without the use of an activation specific marker.

to measure platelet activation, apoptosis, and cell death that may result from passage through the microdevice.

Our first experiment was to see if the chip causes platelet activation. We used CD62p (P-selectin) to measure platelet activation in samples taken from the input and the output wells of the microfluidic device after operation at two different speeds. The output of the device is split into two ports, collecting equal flow from the left and right sides of the device. All output from the device (both output ports) was mixed together for this experiment. The speed in the platelet fractionation array is approximately 500 $\mu$m/s per psi, measured by observing the speed of 200-nm beads through the array. Figure 6.9 shows histograms of CD62p expression for these samples. Normal operating pressure is 2 psi. We used fresh blood collected in ACD anticoagulant. Despite fluctuations, we do not see a significant increase in the fraction of platelets that are CD62p$^+$ after passage through the chip.

Shear forces greater than 280 000 s$^{-1}$ have been shown to destroy, or lyse, red blood cells [64]. Platelet activation, by microparticle formation (release of $\sim$ 100-nm particles into the fluid by the platelets [63]), has been observed at shear rates as low as 10,500 s$^{-1}$, still 5 to 20 times human physiological levels which may be as high as 500 [63] to 2000 s$^{-1}$ [62]. At an operating pressure of 2 psi, the average fluid speed in the platelet fractionation array is 1010 $\mu$m/s. This fluid travels through 6 $\mu$m gaps, so an estimate of the maximum speed would be $1.5 \times 1010 \mu$m/s, since the mean velocity for flow through a slit is 2/3 the maximum velocity. The shear rate is the change in velocity over the distance it changes, $\frac{1.5 \times 1010 \mu\text{m/s}}{3 \mu\text{m}} = 500\text{s}^{-1}$. At 6 psi it would be 1500 s$^{-1}$, and at 15 psi it would be 3800 s$^{-1}$. Thus we do not expect shear-induced activation of platelets until operating pressures of approximately 40 psi.

In a separate experiment we used FITC-conjugated annexin V and propidium iodide to measure apoptosis and cell death, respectively, in samples taken from the input and output wells of the device. Annexin V binds to phospholipid phosphatidylserine

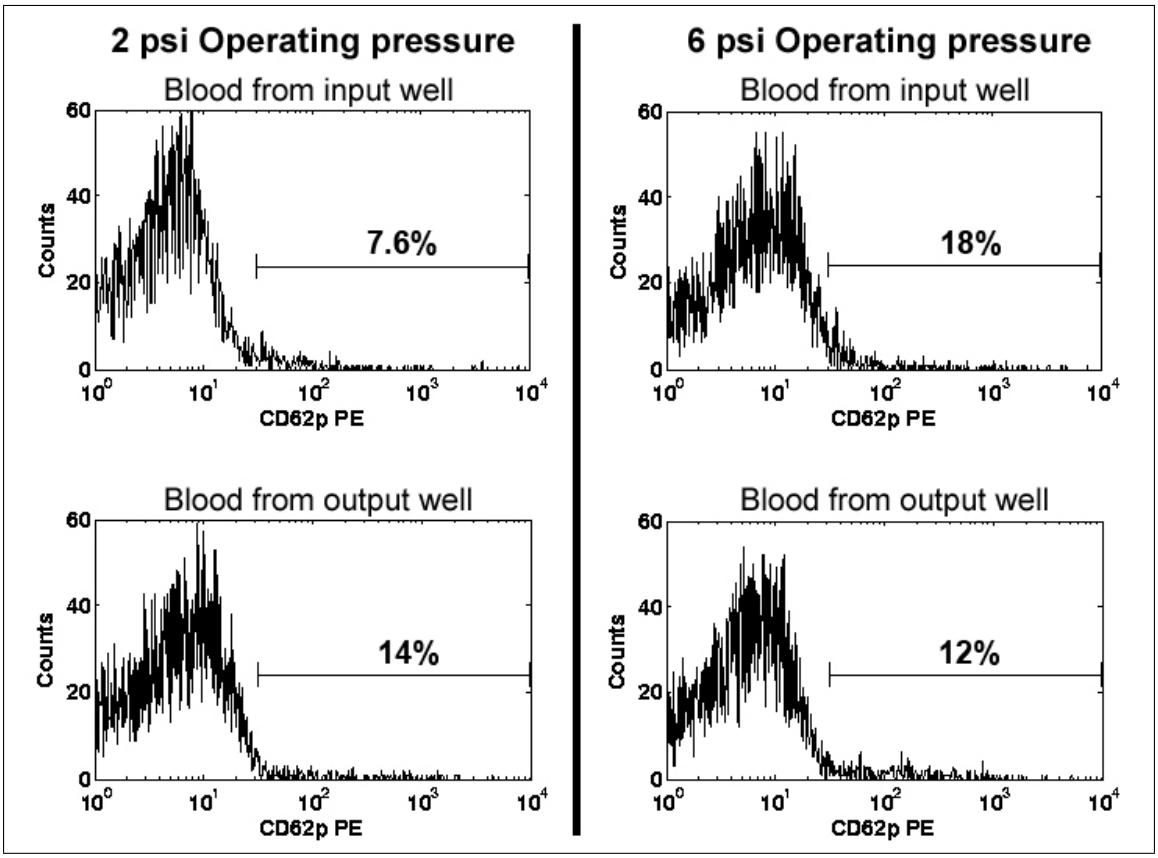


Figure 6.9: Histograms of the platelet activation marker CD62p for platelets that have and have not been run through the device. Blood taken from the input well was not run through the device. Blood from the output well was run through the device. No obvious increase in the fraction of cells expressing CD62p is observed.

(PS) which translocates from the inner to the outer surface of the cell membrane during the early stages of apoptosis. Permeated cells or cell fragments will also have annexin V bound to their inner surfaces. Propidium iodide is a fluorescent dye that binds to DNA, but does not pass through the membranes of live cells. Consequently only dead cells fluoresce. Propidium iodide is sensitive to cell death in white blood cells, whereas annexin V is sensitive to apoptosis in all cells. Blood for this experiment was obtained by finger prick and collected in an EDTA coated tube. Table 6.2 gives a summary of these results.

| Sample ID | Shear Rate $s^{-1}$ | Dead Cells, % | Apoptotic Cells, % |
|---|---|---|---|
| 2 psi input well | 660 | 0.54 | 2.5 |
| 2 psi output well | 660 | 0.66 | 2.3 |
| 15 psi input well | 5000 | 0.50 | 1.7 |
| 15 psi output well | 5000 | 0.55 | 1.6 |

Table 6.2: Percent of cells which are dead and apoptotic before and after passing through the microfluidic device at two different pressures, 2 and 15 psi, corresponding to two different shear rates.

There is no significant increase in the number of dead or apoptotic cells after running through the device for either shear rate, $600s^{-1}$ and $5000s^{-1}$. This is not surprising given that Markou et al. [64] did not see lysis until 5 time greater shear. These two experiments demonstrate that passage through the microfluidic device does not significantly alter platelets or other blood cells.

### 6.3.4 Red blood cell behavior

The behavior of deformable, non-spherical particles in a DLD array is significantly more complex than that of hard spheres. The shear forces, which result from gradients in the fluid velocity around a particle, result in complex motions including tumbling and shape change [85]. This suggests that such particles may appear, in the microfluidic device, to be different sizes depending on their orientation as they pass through the gap. In this section we examine the behavior of non-spherical and highly

deformable red blood cells. The experiments described here were performed on the same devices that the platelet experiments were performed on.

Despite being 7 to 8 microns in diameter and 1.5 to 2 microns thick, red blood cells uneventfully pass through 5 micron diameter capillaries. This is due to their extraordinary deformability, a topic of interest and depth well beyond this discussion. It is known that red blood cells axisymmetrically deform into a parachute shape in capillaries [86]. This shape reduces their maximum diameter to allow them to pass through the capillaries, but also conforms their shape to the parabolic fluid flow profile that exists in any tube.

Nearly all of the red blood cells enter the platelet fractionation array, and behave as approximately 4-micron diameter particles, corresponding to a mean exit position of 490 microns. This is not an obvious result, we had previously guessed that the cells might behave as 2 micron particles, the red blood cell's thin dimension. Perhaps the cells behave in the bump array as they do in capillaries, by conforming to the flow profile. Here the flow profile through most of the gap is parabolic, so perhaps the high velocity in the gap center, relative to the zero velocity at the post folds the disc shaped cell along its long axis, creating a "taco" or "U" shape. Such a change would rely on the cell being easily deformed, and we can see what happens when cells are make more rigid by the addition of a fixative.

Red blood cells in whole blood that had been fixed with paraformaldehyde for 30 minutes behaved as larger particles, exiting the device farther to the right, Fig 6.10. Paraformaldehyde is known to harden cells. By optical microscopy, cells fixed with 1% paraformaldehyde had shrunk from $7.8 \pm 0.6$ to $7.3 \pm 0.4$, a 6% decrease in their large diameter. However the difference in exit position upon fixing with 1% paraformaldehyde correlates to a 1-micron increase in diameter (increase in average exit position of 100 $\mu$m). This is consistent with the hypothesis the the red blood cells navigate the array by conforming to the flow profile and assuming a "taco" or "U" shape.

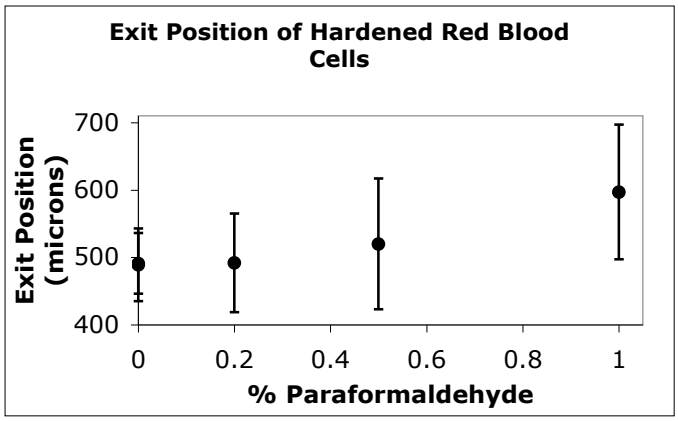


Figure 6.10: Plot of mean exit position for a stream of whole blood vs the % paraformaldehyde used for fixing. The increase in exit position, which correlates with an increase in size, may be a result of decreased deformability of the red blood cells.

This result is in agreement with work by Tsukada et al. [86] who observed that glutaraldehyde-hardened red blood cells and cells from diabetic donors deformed less in microchannels than normal red blood cells.

## 6.4 Things learned the hard way

Platelet morphology is affected by the anticoagulant and method used to collect it, as well as its storage history. It took us too long to realize what experts know, that in order to preserve, as well as possible, the in vivo state of platelets, the blood must be collected from a venal puncture into a citrate anticoagulant. In order to observe the discocyte shape, the blood must be warm (35 to 40$^o$C) and reasonably fresh, less than 2 days old.

The hydrodynamic size of blood taken by capillary finger prick and collected in an EDTA-coated tube has very few (<10%) of the smallest platelets, with a variable and larger number of the largest platelets, many of which are platelet-platelet aggregates (observed by microscopic analysis of diluted blood films). Capillary-finger-prick blood collected in a heparin-coated tube has so many aggregates that is is almost impossible to run in our microdevice, on account of rapid clogging. I was not able to obtain citrate-coated capillary blood collection tubes.

Venal blood collected in an EDTA tube is similar to the EDTA capillary blood

sample, but without the aggregates. Upon 2 days of cold storage no significant changes occur. Venal blood collected in an heparin tube is broadly distributed over the hydrodynamic size range, with 15% of platelets being less than 2.4 microns and approximately 25% being larger than 4.8 microns. After 2 days of cold storage the platelets in the heparin sample are reduced in size, with as much as 40% being less than 2.4 microns. These platelets or platelet fragments also bind much less CD41 and can be difficult to see. According to conversations with Dr. James White, a platelet expert at the University of Minnesota, heparin anticoagulated-platelets, stored cold for 2 days permanenetly convert to spherocytes. Thus using heparin for platelet studies, even with venal blood, is not recommended

## 6.5 Summary

In this chapter we have shown evidence that a microfluidic device can distinguish between blood with activated platelets from that which is not activated, without use of an activation specific cell-label. This is possible because activated and non-activated platelets have different shapes and the device causes cells of different shapes to take different paths. This is especially significant because chemicals that report activation status do not respond equally to all routes to activation [64]. We also showed that the device induced little or no cell death or apoptosis and little or no platelet activation. This device was also able to measure a change in red blood cells caused by exposure to the fixative paraformaldehyde. These diagnostic measures may be useful in a wide range of medical procedures such as diagnosis of platelet function or viability and diagnosing and perhaps treating red blood cell disorders by the selective removal of undesirable cells.

# Chapter 7

# Conclusion

## 7.1 Summary

For fun or curiosity, or for the pursuit of a better life, humans have built tools. Today, the tool designers are called engineers, and it is their calling to make useful objects. The engineer's interaction with biology can be daunting and exciting, as he or she is frustrated by an organism or a cells strange behavior and at the same time senses the potential for new insight and new tools. This describes my experience designing, and testing devices that sort and separate cells on a micro scale.

We have shown a method for separating cells once magnetic beads have been attached to them. Of all the chapters, this one took the most amount of time. I first had to learn how to design into the chips and into the external pluming, features that made precise and sensitive control of the fluid flow possible. Then there were many other challenges, that for the most part were overcome by trial and error. This method of separation would be most useful in carrying a labeled and captured cell to a sensor or analysis system, but the greatest challenge is preventing unwanted cell-surface adhesion.

The method for particle separation by size, invented by L.R. Huang in 2003 [5],

was very exciting and had obvious application to blood cell separation. A model was developed to explain what would happen when the row shift was varied. These ideas have been tested many times over. A few other parameters were briefly investigated, but not with such rigor. The range of particle sizes that could be separated on a chip was increased by cascading multiple arrays and including alternate, non-clogging paths for larger particles. This device was successful at removing all cells including platelets from blood plasma without clogging. However, there is likely to be significant diffusional mixing between the plasma and the buffer.

The size separation method can also be used to measure size, where position correlates with size to give a sort of size spectroscopy. We showed two devices where this was used: one that measured the size of white blood cells, and one that measured the size of platelets and red blood cells. Size measurements of white blood cells may assist in the earlier detection of diseases like cancer, and size/morphology measurements may assist in the diagnosis of bleeding and clotting disorders. Both technologies are however up against long established technologies such as flow cytometry.

Biology is about four billion years old, and its age is reflected in its complexity. Biology is more complex and sophisticated than most anything we can comprehend. To capture this complexity, the tools that humanity uses to quantify biology are necessarily diverse. We might one day have an all-in-one medical diagnostic device, but it too will be more complex and sophisticated than most anything we can comprehend.

These cell separation methods are a tiny piece of the microfluidic field, which itself is a small field of research. Nevertheless, the small contributions made here will hopefully be valuable and useful to someone, though I hope that the contributions I make to the lives of the people around me will amount to much more.

# Appendix A

# Publications and Conference Presentations Arising From This Dissertation

## Journal articles

1. D. W. Inglis, J. A. Davis, T. J. Zieziulewicz, D. A. Lawrence, R. H. Austin and J. C. Sturm, "Determining blood cell size using deterministic hydrodynamics," submitted to Journal of Immunological Methods, Oct 2006.

2. J. A. Davis, D. W. Inglis, K. J. Morten, D. A. Lawrence, L. R. Huang, S. Y. Chou, J. C. Sturm, R. H. Austin, "Deterministic hydrodynamics: Taking blood apart," PNAS **103**, 14779–14787 (2006).

3. D. W. Inglis, J. A. Davis, R. H. Austin and J. C. Sturm, "Critical particle size for fractionation by deterministic lateral displacement," Lab Chip **6**, 655–658 (2006).

4. D. W. Inglis, R. Riehn, R. H. Austin and J. C. Sturm, "Continuous microflu-

idic immunomagnetic cell separation," Applied Physics Letters **85**, 5093–5095 (2004).

## Conference proceedings

1. D. W. Inglis, R. Riehn, J. C. Sturm and R. H. Austin, "Microfluidic high gradient magnetic cell separation," Journal of Applied Physics **99**, 08K101 (2006). Proceedings to the 2005 Magnetism and Magnetic Materials conference in San Jose California.

## Conference Presentations

1. D. W. Inglis, J. C. Sturm and R. H. Austin, "Railroading cells, microfluidic magnetic cell separation using ferromagnetic stripes," 2006 APS March Meeting, Baltimore MD.

2. D. W. Inglis, R. Riehn, J. C. Sturm and R. H. Austin, "Microfluidic high gradient magnetic cell separation," Presented in November 2005 at the Magnetism and Magnetic Materials conference in San Jose California.

3. D. W. Inglis, R. Riehn, J. C. Sturm and R. H. Austin, "Continuous microfluidic immunomagnetic cell separation," 2005 APS March Meeting, Los Angeles CA.

# Appendix B

# Protocals

## B.1 Photolithography

**Standard procedure**

Clean mask start with a clean substrate prebake 5 min 110 celcius on hotplate spin HMDS 4000rpm 40s spin AZ 5214 4000rpm 40s thickness should be 1.4um soft bake 95 celcius for 1 minute exposure 2.0W on MA6 for 35 to 40 s use hard contact for sub 10 micron features. develop 1:1.2, MIF 312:water for 30s to 1 minute depending on amount of PR to remove constantly stir the developer with the wafer rinse thoroughly rinse thoroughly again with tweezers not at the top of wafer dry hard bake 3-5 minutes at 95 celcius

**Image reversal**

Clean mask start with a clean substrate prebake 5 min 110 celcius on clean hotplate with no glass slides) spin hmds 4000rpm 40s spin AZ 5214 4000rpm 40s thickness should be 1.4um soft bake 95 celcius for 1 minute exposure 2.0W on MA6 for 30 s using your mask. use hard contact for sub 10 micron features short hard bake, 30s, 110 Celcius flood exposure, use a blank mask plate, 30s at 2.0 W on MA6. develop 1:1, MIF 312:water for 30s constantly stir the developer with the wafer rinse thoroughly

rinse thoroughly again with tweezers not at the top of wafer dry hard bake 3-5 minutes at 95 celcius

## B.2 CMP

This work was carried out at the Cornell Nanofabrication Facility on the Strasbaugh 6EC Chemical Mechanical Polishing Tool. For Nnckel polishing use the MSW2000 Tungsten slurry, on an IC1400 pad. 3 minutes of the standard process to remove 5 microns of electroplated nickel. 12 minutes of the standard process to remove 5 microns of sputtered nickel.

To achieve a more uniform polishing rate over the wafer surface it is useful use "dummy" features. dummy features are features, similar to the ones that you are trying to fabricate, distributed over the wafer surface. This increases the polishing rate in those areas, and thus creates a final product that is flatter.

## B.3 DRIE etching

'Deep' silicon etch on the Plasmatherm 720 in the PRISM clean room SF6 at 60 sccm CCl2F2 at 15 sccm pressure:100mTorr power: 200W selectivity Si:PR 7:1 0.8um/min etch rate when etching 30% of a 4" wafer. rate can vary a great deal Silicon nitride can also be used as an etch mask to get another few microns of depth.

## B.4 Sandblasting

sandblasting was done to every single device backplane used. Others have tried to cut holes in the PDMS layer for fluid connection, but this often leads to loose pieces of PDMS that clog the device. Do the sandblasting step as early in the fabrication as possible, it's dirty. It can even be done before photolithography, but it not ideal.

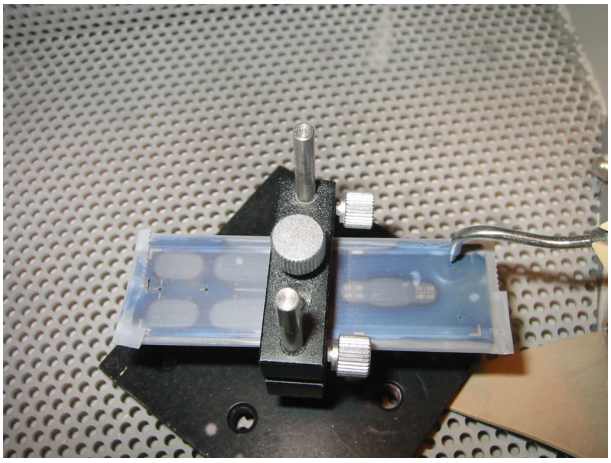

Figure B.1: Photograph of a substrate to be sandblasted held in a chuck. The sandblasting sprayer is to the right.

I used a small dental sandblaster to cut small (0.5-1 mm) holes in silicon wafer pieces. To do this, first cleave a wafer into appropriately sized pieces, then cover all surfaces with Scotch tape. Avoid having a seam at the spot where you will sandblast. Using a sharp permanent felt tipped marker make an X where you want the hole to be. It is best to have something to mount the wafer piece in during sandblasting. I used the chuck shown in Figure B.1. The nozzles of the sprayers should be 1 to 5 mm above the piece to be sandblasted.

## B.5 Magnetic cell labeling

100 microL of whole blood 20 microL of antibody conjugated microbeads from Miltenyi Biotec mix and let stand for 15 minutes at 9 Celcius.

## B.6 Fluorescent cell labeling

### Hoechst

Hoechst is a vital nucleic dye, that must be passed to the nucleus. Once there is increases in brightness. 100 microL of whole blood (EDTA or heparin anticoagulant) 1 microL of 10 mg/mL stock Hoechst 33342 solution. mix and incubate for 15 minutes

at 37 Celcius.

### Fluoescent antibodies

These labels typically bind to a cell wall. I have used the fluorescent molecules: PE (phycoerythrin) [560-¿575 nm] and, FITC (fluorescein) [495-¿510] conjugated to various antigens, such as CD3, CD8, CD14, CD16, CD41 and CD62p. PE is brighter than FITC, but both will photo-bleach. Ebiosciences.com manufactures and sells these, pre-conjugated and ready to use in liquid form.

For whole blood, 15 microL whole blood 3 microL of the manufacturers antibody mixture. mix well, and let stand for 20 minutes are room temperature. We have seen labeling with as little as 0.3 microliters per 15 microliters blood.

In many cases, unbound dye molecules will have to be washed away: centrifuge at $\sim 1500\times$g for 1 minute pipette off supernatant re-suspend with PBS or other suitable buffer to the desired volume. vortex again to break up the pellet.

## B.7 Silane coating

I do this on the device substrates to reduce cellular adhesion, and to prevent PDMS from sticking to a master mold.

Start with a very clean substrate, I recommend an H2SO4 – H2O2 clean then HF dip. Grow a thin oxide: 3 hours at 1000 Celsius in a atmospheric gases Generate dangling bonds: 1 minute oxygen plasma. immediately transfer to silane coating bell jar. pipette 50 microL of TridecaFluoro –1,1,2,2 – tetrahydroctyl Trichlorosilane (Gelest Inc. SIT 8174.0 - 10GM) into a small disposable dish in the bottom of the bell jar. Do this in a fume hood evacuate to 25 inches of mercury and seal the jar. Let stand for at least 2 hours. Remove from the bell jar (in the fume hood). Bake for at least 2 hours in an oven at 65 to 95 Celcius Wash with acetone then isopropanol

to remove any unbound molecules.

Substrates should now be very hydrophobic.

## B.8 Making silicone molds

Mix PDMS (RTV 615-a, GE silicones), 10 parts PDMS with 1 part cross-linking agent. A total of 15 grams will completely coat a wafer, 4 grams will do for making PDMS coated glass slides. place in a bell jar and evacuate. Maintain vacuum until all the bubbles on the surface of the PDMS are gone, about 1 hour.

Remove from bell jar and immediately pour over fluoro-silane treated master mold features. You may wish to squish the PDMS with a glass slide at this time. Wait for any irregularities in the pattern to disappear before curing. The irregularities may be caused by bubbles, trapped at the bottom of the features, which will eventually dissolve.

Cure in a 70 Celcius oven for 2 hours.

The PDMS-glass slide daughter mold can be removed from the master mold by prying the two layers apart using a razor blade and a steady hand. Be patient, and allow the molds to separate slowly.

## B.9 Cell fixing

Cells, including whole blood can be fixed by mixing them with paraformaldehyde to result in a 0.5 to 1% solution of paraformaldehyde. Glutaraldehyde is more commonly used for fixing cells because it completes the fixing procedure in less time, but I only have experience with paraformaldehyde.

To prepare a 4% stock solution: weight out 0.4 g of paraformaldehye, transfer to a 15 ml tube. add 8 ml of DI water add 5 microL of 1 M NaOH heat, cap on, to 70 Celcius, mixing frequently until completely solubilized, the solution should be clear

(10-30 min). Allow to cool on ice. Adjust volume to 9 ml with DI water add 1ml of 10x PBS (10 times concentrated phosphate buffered saline) Filter the solutions using a 0.2 micron nylon syringe filter.

Use the fixative at room temperature, and allow 30 minutes for fixing to occur.

# Bibliography


[1] A. Manz, N. Graber, and H. M. Widmer, "Miniaturized total chemical analysis systems: A novel concept for chemical sensing," *Sensors and Actuators B*, vol. 1, pp. 244–248, 1990.

[2] M. B. Elowitz, A. J. Levine, E. D. Siggia, and P. S. Swain, "Stochastic gene expression in a single cell," *Science*, vol. 297, pp. 1183–1186, 2002.

[3] A. J. Tudos, G. A. J. Besselink, and R. B. M. Schasfoort, "Trends in miniaturized total analysis systems for point-of-care testing in clinical chemistry," *Lab on a Chip*, vol. 1, pp. 83–95, 2001.

[4] M. Toner and D. Irimia, "Blood-on-a-chip," *Annu. Rev. Biomed. Eng.*, vol. 7, pp. 77–103, 2005.

[5] L. R. Huang, E. C. Cox, R. H. Austin, and J. C. Sturm, "Continuous particle separation through deterministic lateral displacement," *Science*, vol. 304, pp. 987–990, May 2004.

[6] H. M. Shapiro, *Practical Flow Cytometry*. Hoboken, New Jersey: John Wiley & Sons, Inc, 2003.

[7] S. Miltenyi, W. Müller, W. Weichel, and A. Radbruch, "High gradient magnetic cell separation with MACS," *Cytometry*, vol. 11, pp. 231–238, 1990.

[8] M. Nakamura, K. Decker, J. Chosy, K. Comella, K. Melnik, L. Moore, L. C. Lasky, M. Zborowski, and J. C. Chalmers, "Separation of a breast cancer cell line from human blood using a quadrupole magnetic flow sorter," *Biotechnol. Prog.*, vol. 17, pp. 1145–1155, 2001.

[9] H. Taubert, K. Blmke, U. Bilkenroth, A. Meye, A. Kutz, F. Bartel, C. Lautenschläger, E. J. Ulbrich, N. Nass, H. Holzhausen, H. Koelbl, and A. Lebrecht, "Detection of disseminated tumor cells in peripheral blood of patients with breast cancer: correlation to nodal status and occurrence of metastases," *Gynecologic Oncology*, vol. 92, pp. 256–261, 2004.

[10] D. Melville, F. Paul, and S. Roath, "Direct magnetic separation of red cells from whole blood," *Nature*, vol. 255, p. 706, 1975.

[11] R. S. Molday, S. P. S. Yen, and A. Rembaum, "Applications of magnetic microspheres in labeling and separation of cells," *Nature*, vol. 268, pp. 437–438, 1977.

[12] K. Han and A. B. Frazier, "Continuous magnetophoretic separation of blood cells in a microdevice format," *Journal of Applied Physics*, vol. 96, no. 10, pp. 5797–5802, 2004.

[13] K. Han and A. B. Frazier, "Paramagnetic capture mode magnetophoretic microseparator for high efficiency blood cell separations," *Lab Chip*, vol. 6, pp. 265–273, 2006.

[14] D. W. Inglis, R. Riehn, R. H. Austin, and J. C. Sturm, "Continuous microfluidic immunomagnetic cell separation," *Applied Physics Letters*, vol. 85, pp. 5093–5095, 2004.

[15] L. Sakhnini and R. Khuzaie, "Magnetic behavior of human erythrocytes at different hemoglobin states," *Eur. Biophys. J.*, vol. 30, pp. 467–470, 2001.

[16] L. Sakhnini, "Magnetic measurements on human erythrocytes: normal, beta thalassemia major, and sickle," *Journal of Applied Physics*, vol. 93, pp. 6721–6723, 2003.

[17] M. Takayasu, N. Duske, S. R. Ash, and F. J. Friedlaender, "HGMS studies of blood cell behavior in plasma," *IEEE Transactions on Magnetics*, vol. MAG-82, pp. 1520–1522, 1982.

[18] D. Melville, F. Paul, and S. Roath, "Fractionation of blood components using high gradient magnetic separation," *IEEE Transactions on Magnetics*, vol. MAG-18, pp. 1680–1685, 1982.

[19] M. D. Graham, "Efficiency comparison of two preparative mechanisms for magnetic separation of erythrocytes from whole blood," *Journal of Applied Physics*, vol. 52, pp. 2578–2580, 1981.

[20] M. Takayasu, D. R. Kelland, and J. V. Minervini, "Continuous magnetic separation of blood components from whole blood," *IEEE transactions on applied superconductivity*, vol. 10, pp. 927–930, 2000.

[21] F. Paul, D. Melville, S. Roath, and D. C. Warhurst, "A bench top separator for malarial parasite concentration," *IEEE Transactions on Magnetics*, vol. MAG-17, pp. 2822–2824, 1981.

[22] F. Paul, S. Roath, d. Melville, D. C. warhurst, and J. O. S. Osisanya, "Separation of malaria-infected erythrocytes from whole blood:use of a selective high-gradient magnetic separation technique," *Lancet*, vol. 2, pp. 70–71, 1981.

[23] C. S. Owen and N. L. Sykes, "Magnetic labeling and cell sorting," *Journal of Immunological Methods*, vol. 73, pp. 41–48, 1984.

[24] S. Sieben, C. Bergemann, A. Lübbe, B. Brockmann, and D. Rescheleit, "Comparison of different particles and methods for magnetic isolation of circulating tumor cells," *Journal of Magnetism and Magnetic Materials*, vol. 225, pp. 175–179, 2001.

[25] J. C. Chalmers, M. Zborowski, L. Sun, and L. Moore, "Flow through immunomagnetic cell separation," *Biotechnol. Prog.*, vol. 14, pp. 141–148, 1998.

[26] A. B. Kantor and I. Gibbons, *Cell Separation Methods and Applications: Chapter 8. Magnetic Cell Sorting with Colloidal Superparamagnetic Particles*. New York: Marcel Dekker, Inc, 1998. Book editors are D. Recktenwald and A. Radbruch.

[27] A. G. Tibbe, B. G. d. Grooth, J. Greve, G. J. Dolan, C. Rao, and L. W. Terstappen, "Magnetic field design for selecting and aligning immunomagnetic labeled cells," *Cytometry*, vol. 47, pp. 163–172, 2002.

[28] K. E. McCloskey, J. J. Chalmers, and M. Zborowski, "Magnetic cell separation: characterization of magnetophoretic mobility," *Anal. Chem.*, vol. 75, pp. 6868–6874, 2003.

[29] C. H. Ahn, M. G. Allen, W. Trimmer, Y. Jun, and S. Erramilli, "A fully integrated micromachined magnetic particle separator," *Journal of Microelectromechanical Systems*, vol. 5, pp. 151–158, 1996.

[30] N. Pekas, M. Granger, M. Tondra, A. Popple, and M. D. Porter, "Magnetic particle diverter in an integrated microfluidic format," *Journal of Magnetism and Magnetic Materials*, vol. 293, pp. 584–588, 2005.

[31] N. Pamme and A. Manz, "On-chip free-flow magnetophoresis: continuous flow separation of magnetic particles and agglomerates," *Anal. Chem.*, vol. 76, pp. 7250–7256, 2004.

[32] E. Mirowski, J. Moreland, and S. E. Russek, "Integrated microfluidic isolation platform for magnetic particle manipulations in biological systems," *Applied Physics Letters*, vol. 84, pp. 1786–1788, 2004.

[33] T. Deng, M. Prentiss, and G. M. Whitesides, "Fabrication of magnetic microfiltration system using soft lithography," *Applied Physics Letters*, vol. 80, pp. 461–463, 2002.

[34] J. Choi, C. H. Ahn, S. Bhansali, and H. Henderson, "A new magnetic bead-based, filterless bio-separator with planar electromagnetic surfaces for integrated bio-detection systems," *Sensors and Actuators B*, vol. 68, pp. 34–39, 2000.

[35] M. Berger, J. Castelino, R. Huang, M. Shah, and R. H. Austin, "Design of a microfabricated magnetic cell separator," *Electrophoresis*, vol. 22, pp. 3883–3892, 2001.

[36] V. Furdui and D. J. Harrison, "Immunomagnetic T cell capture from blood for PCR analysis using microfluidic system," *Lab Chip*, vol. 4, pp. 614–618, 2004.

[37] H. Lee, A. M. Purdon, and R. M. Westervelt, "Manipulation of biological cells using a microelectromagnetic matrix," *Applied Physics Letters*, vol. 85, pp. 1063–1065, 2004.

[38] S. Y. Chou, "Patterned magnetic nanostructures and quantized magnetic disks," *Proceedings of the IEEE*, vol. 85, pp. 652–671, 1997.

[39] M. Pelton, K. Ladavac, and D. G. Grier, "Transport and fractionation in periodic potential-energy landscapes," *Physical Review E*, vol. 70, p. 031108, 2004.

[40] N. Darnton, O. Bakajin, R. Huang, B. North, J. O. Tegenfeldt, E. C. Cox, J. Sturm, and R. H. Austin, "Hyrdrodynamics in $2\frac{1}{2}$ dimensions: making jets in a plane," *Journal of Physics: Condensed Matter*, vol. 13, pp. 4891–4902, 2001.

[41] A. Bikoue, F. George, P. Poncelet, M. Mutin, G. Janossy, and J. Sompol, "Quantitative analysis of leukocyte membrane anitgen expression: Normal adult values," *Cytometry*, vol. 26, pp. 137–147, 1996.

[42] A. Bikoue, G. Janossy, and D. Barnett, "Stabilised cellular immuno-fluorescence assay: CD45 expression as a calibrated standard for human leukocytes," *Journal of Immunological Methods*, vol. 266, pp. 19–32, 2002.

[43] T. McPherson, A. Kidane, I. Szleifer, and K. Park, "Prevention of protein adsorption by tethered poly(ethylene oxide) layers: experiments and single-chain mean-field analysis," *Langmuir*, vol. 14, pp. 176–186, 1998.

[44] A. Winkelstein, R. A. Sacher, S. S. Kaplan, and G. T. Roberts, *White Cell Manual*. F.A. Davis, 5th ed., 1998.

[45] M. Tondra, M. Porter, and R. J. Lipert, "Model for detection of immobilized superparamagnetic nanosphere assay labels using giant magnetoresistive sensors," *Journal of Vacuum Science & Technology A: Vacuum, Surfaces and Films*, vol. 18, pp. 1125–1129, 2000.

[46] N. Wang and D. E. Ingber, "Probing transmembrane mechanical coupling and cytomechanics using magnetic twisting cytometry," *Biochem Cell Biol*, vol. 73, pp. 327–335, 1995.

[47] J. A. Davis, D. W. Inglis, K. M. Morton, D. A. Lawrence, L. R. Huang, S. Y. Chou, J. C. Sturm, and R. H. Austin, "Deterministic hydrodynamics: taking blood apart," *Proc. Nat. Acad. Sci. (USA)*, vol. 103, pp. 14779–14784, 2006.

[48] J. P. Brody, P. Yager, R. E. Goldstein, and R. H. Austin, "Biotechnology at low Reynolds numbers," *Biophys. J.*, vol. 71, pp. 3430–3441, 1996.

[49] E. Hecht and A. Zajac, *Optics*. Addison-Wesley, 1975.

[50] F. M. Laurencet, A. Doucet, V. Lydiate, M. Jacquier, B. Mermillod, S. Andersen, and B. Chapuis, "Quality evaluation of plateletpheresis using the new AMICUS (Baxter) cell separator: Evolution of CD62 expression," *Journal of Clinical Apheresis*, vol. 13, pp. 47–55, 1998.

[51] S. Urbanits, A. Griesmacher, G. Hopfinger, G. Stockhammer, A. Karimi, M. M. Müller, E. Pittermann, and W. Grisold, "FACS analysis – a new and accurate tool in the diagnosis of lymphoma in the cerebrospinal fluid," *Clinica Chimica Acta*, vol. 317, pp. 101–107, 2002.

[52] V. VanDelinder and A. Groisman, "Separation of plasma from whole human blood in a continuous cross-flow in a molded microfluidic device," *Anal. Chem.*, vol. 78, pp. 3765–3771, 2006.

[53] S. Yang, A. Undar, and J. D. Zahn, "A microfluidic device for continuous, real time blood plasma separation," *Lab Chip*, vol. 6, pp. 871–880, 2006.

[54] M. Y. J. Takagi, M. Yamada and M. Seki, "Continuous particle separation in a microchannel having asymmetrically arranged multiple branches," *Lab Chip*, vol. 5, pp. 778–784, 2005.

[55] M. Nakashima, M. Yamada, , and M. Seki, "Pinched flow fractionation (PFF) for continuous particle separation in a microfluidic format," *Proceedings of IEEE MEMS*, pp. 33–36, 2004.

[56] M. Yamada and M. Seki, "Microfluidic particle sorter employing flow splitting and recombining," *Anal. Chem.*, vol. 78, pp. 1357–1362, 2006.

[57] Landau and Lifshitz, *Fluid Mechanics*. Butterworth-Heinemann, second ed., 1995.

[58] H. C. Berg, *Random Walks in Biology*. Princeton University Press, 1993.

[59] E. R. Dufresne, T. M. Squires, M. P. Brenner, and D. G. Grier, "Hydrodynamic coupling of two brownian spheres to a planar surface," *Physical Review Letters*, vol. 85, pp. 3317–3320, 2000.

[60] T. E. Creighton, *Proteins*. W. H. Freeman and Company, second ed., 1993.

[61] D. E. Gray, *American Institute of Physics Handbook*. McGraw-Hill, third ed., 1972.

[62] R. A. F. Jr., *Nanomedicine*, vol. I, Basic Capabilities. Landes Bioscience, 1999.

[63] P. Holme, U. Orvim, M. J. Hamers, N. O. Solum, F. R. Brosstad, R. M. Barstad, and K. S. Sakariassen, "Shear-induced platelet activation and platelet microparticle formation at blood flow conditions as in arteries with a severe stenosis," *Arterioscler Thromb Vasc Biol*, vol. 4, pp. 646–653, 1997.

[64] C. P. Markou, U. M. Marzec, J. A. Chinn, F. Hirt, and S. R. Hanson, "Shear induced platelet activation," *Proceedings of he First Joint BMES/EMBS Conference, Serving Humanity, Advancing Technology*, p. 770, 1999. Oct 13-16, Atlanta GA, USA.

[65] M. Eisenstein, "Divide and conquer," *Nature*, vol. 441, pp. 1179–1185, 2006.

[66] H. M. Shapiro and N. G. Perlmutter, "Personal cytometers: slow flow or no flow?," *Cytometry Part A*, vol. 69, pp. 620–630, 2006.

[67] S. Zheng, R. Yung, Y. Tai, and H. Kasdan, "Deterministic lateral displacement MEMS device for continuous blood cell separation," *Proceedings of IEEE MEMS*, pp. 851–854, 2005.

[68] S. Zheng, Y. Tai, and H. Kasdan, "MEMS device for continuous blood cell separation," *Proceedings of $\mu TAS$*, pp. 385–387, 2005.

[69] X. Zhang, J. M. Cooper, P. B. Monaghan, and S. J. Haswell, "Continuous flow separation of particles within an asymmetric microfluidic device," *Lab Chip*, vol. 6, pp. 561–566, 2006.

[70] M. Yamada, M. Nakashima, and M. Seki, "Pinched flow fractionation: continuous size separation of particles utilizing a laminar flow profile in a pinched microchannel," *Anal. Chem.*, vol. 18, pp. 5465–5471, 2004.

[71] D. Huh, W. Gu, Y. Kamotani, J. B. Grotberg, and S. Takayama, "Microfluidics for flow cytometric analysis of cells and particles," *Physiol. Meas.*, vol. 26, pp. R73–R98, 2005.

[72] C. Simonnet and A. Groisman, "High-throughput and high-resolution flow cytometry in molded microfluidic devices," *Anal. Chem.*, vol. 78, pp. 5653–5663, 2006.

[73] D. W. Inglis, J. A. Davis, T. J. Zieziulewicz, D. A. Lawrence, R. H. Austin, and J. C. Sturm, "Determining blood cell size using microfluidic hydrodynamics," *J. Immunol. Meth.*, 2007. submitted oct 2006.

[74] Dacie and Lewis, *Practical Haematology*. London: Churchill Livingstone, 2001. Edited by S. M. Lewis, B. J. Bain and I. Bates.

[75] M. M. Frojmovic and R. Panjwani, "Geometry of normal mammalian platelets by quantitative microscopic studies," *Biophysical Journal*, vol. 16, pp. 1071–1089, 1976.

[76] M. M. Frojmovic, J. G. Milton, J. P. Caen, and G. Tobelemn, "Platelets from giant platelet syndrome (bss) are discocytes and normal sized," *Journal of laboratory and clinical medicine*, vol. 91, pp. 109–116, 1978.

[77] J. B. Miale, *Laboratory Medicine Hematology*. Saint Louis: The C. V. Mosby Company, 1977.

[78] P. Harrison, "Platelet function analysis," *Blood Reviews*, vol. 19, pp. 111–123, 2005.

[79] A. S. Kantak, B. K. Gale, Y. Lvov, and S. A. Jones, "Microfluidic platelet function analyzer for shear-induced platelet activation studies," *2nd Annual International IEEE-EMBS Special Topic Conference on Microtechnologies in Medicine & Biology*, 2002. Madison, Wisconsin USA.

[80] Y. Martin, A. Bannari, and P. Vermette, "Instrument and technique for the *in vitro* screening of platelet activation from whole blood samples," *Review of Scientific Instruments*, vol. 78, p. 054302, 2007.

[81] J. G. White and G. H. R. Rao, "Microtubule coils *versus* the surface membrane cytoskeleton in maintenance and restoration of platelet discoid shape," *American Journal of Pathology*, vol. 152, pp. 597–609, 1998.

[82] V. Leytin, M. Mody, J. W. Semple, B. Garvey, and J. Freedman, "Flow cytometric parameters for characterizing platelet activation by measuring p-selectin (cd62) expression: Theoretical consideration and evaluation in thrombin-treated platelet populations," *Biochemical and Biophysical Research Communications*, vol. 269, pp. 85–90, 2000.

[83] M. B. Zucker and J. Borrelli, "Reversible alterations in platelet morphology produced by anticoagulants and by cold," *Blood*, vol. 9, pp. 602–608, 1954.

[84] B. Bull and M. B. Zucker, "Changes in platelet volume produced by temperature, metabolic inhibitors, and aggregating agents.," *Proc. Soc. Exp. Biol. Med.*, vol. 120, pp. 296–301, 1965.

[85] H. Noguchi and G. Gompper, "Fluid vesicles with viscous membranes in shear flow," *Physical Review Letters*, vol. 93, p. 258102, 2004.

[86] K. Tsukada, E. Sekizuka, C. Oshio, and H. Minamitani, "Direct measurement of erythrocyte deformability in diabetes mellitus with a transport microchannel capillary model and high-speed video camera system," *Microvascular Research*, vol. 61, pp. 231–239, 2001.